OPEN ACCESS

University of BRISTOL

Peer reviewed version

Link to published version (if available):
10.1002/eqe.2778

Link to publication record in Explore Bristol Research
PDF-document

University of Bristol - Explore Bristol Research
General rights

Influence of frequency-dependent soil-structure interaction on the fragility of R/C bridges

Nikolaos Lesgidis[1], Anastasios Sextos[1,2] and Oh-Sung Kwon[3]

[1] Department of Civil Engineering, Aristotle University Thessaloniki, Greece

[2] Department of Civil Engineering, University of Bristol, United Kingdom

[3] Department of Civil Engineering, University of Toronto, Canada.

SUMMARY

Bridge performance under earthquake loading can be significantly influenced by the interaction between the structure and the supporting soil. Even though the frequency dependence of the above interaction has long been documented, the simplifying assumption that the dynamic stiffness is dominated by the mean or predominant excitation frequency is still commonly made, primarily due to the associated numerical difficulties when the analysis has to be performed in the time domain. This study makes use of the advanced Lumped Parameter (LP) models recently developed [1] in order to quantify the impact of the above assumption on the predicted fragility of bridges. This is achieved by comparing the predicted vulnerability for the case of a reference, well studied, actual bridge using both conventional, frequency-independent, Kelvin Voigt Models and the aforementioned LP formulation. Analyses results demonstrate that the more refined consideration of frequency dependence of soil-structure interaction at the piers and the abutments of a bridge, not only leads to different probabilities of failure for given intensity measures but also to different hierarchy and distribution of damage within the structure for the same set of earthquake ground motions even if the overall probability of exceeding a given damage state is the same. The paper concludes with the comparative assessment of the above effect for different soil conditions, foundation configurations and ground motion characteristics along with the relevant analysis and design recommendations.

Keywords: bridges, soil-structure interaction, lumped parameter model, fragility analysis.

1. INTRODUCTION

Seismic risk assessment of bridge structures within a road network is considered an essential tool for the appropriate management of the network as a whole, as well as the effective mitigation of the direct and indirect socioeconomic loses that may arise on the occurrence of a significant earthquake event. Bridges are essentially the most critical components of such a highway grid as the associated uncertainty in the prediction of their fragility directly propagates to the network level. Any simplification therefore on the reliability chain of defining the interplay between the earthquake excitation and the dynamic properties of the soil – bridge system may affect the estimation of the network seismic risk in question.

One of key aspects in the aforementioned reliability chain is the numerical simulation of soil-structure interaction at every pier-foundation and abutment-embankment support of the bridge. As it has been well documented in the literature, neglecting or oversimplifying the complex dynamic impedance at the interfaces between the structure and the foundation may lead to misleading prediction of the bridge behavior under severe earthquake loading [2]. Most importantly,

it is well established that the nature of soil-structure interaction is inherently frequency-dependent [3–8] and as such, the complex dynamic impedance matrix is affected by the frequency content of the incoming (uniform or non-uniform [9]) seismic motion at each bridge support, particularly as soil responds inelastically. Naturally therefore, the level of numerical refinement and approach adopted to consider SSI effects is a crucial decision with significant implications in both design and assessment of bridges.

As observed in the literature, different SSI simulation methods have been incorporated in the framework of seismic risk assessment of bridges for both long structures and overpasses. The truncated FEM simulation of the entire soil domain–structure system can provide a reliable representation and account for the dynamic properties and failure mechanisms of the semi-infinite soil, thus permitting the assessment of the entire system [10,11]. The importance of accounting for the inelastic response of the soil domain for assessing the seismic response of soil-bridge systems has also been highlighted in the literature [12,13]. The actual dilemma faced however, is whether frequency dependence of soil-structure interaction is of primary importance (hence, appropriate impedance functions have to be used, inevitably, in the framework of analysis in the frequency domain), or the material and geometric nonlinearities of the soil-bridge system are deemed more important thus dictating analysis in the time domain. In latter case, the holistic FEM approach may be further prohibitive as it is computationally expensive, thus becoming practically prohibitive for vulnerability analyses, which require an extensive nonlinear analysis sample.

In the light of the aforementioned limitations, the most common approach is to sacrifice the modeling refinement in terms of subsoil domain size and frequency-dependence by system substructuring and primary focus on refined models tailored to capture damage at the structural and foundation components, as well as due to geometric nonlinearities that arise from gap closure and stopper activation. Along these lines, soil-structure interaction is considered through the use of either a lumped spring [14,15] or the long established (but also frequency-independent) Kelvin-Voigt model [16].

The Lumped Parameter modeling method (LP method) [3,17–21] is a computationally viable answer to address the above compromise, however, a number of accuracy and instability issues hinder its unconditional application. To this end, an alternative modeling procedure has been developed recently [1] proposing an accurate, globally stable and feasible way to consider frequency-dependent SSI phenomena independently of the problem size, nonlinearity and FEM software used. This paper proceeds further and aims to define the circumstances under which a thorough frequency-dependent approach is essential for the seismic risk assessment of a bridge structure. The aforementioned investigation is performed at the level of system fragility for a reference overpass bridge under different combinations of soil properties, earthquake characteristics and foundation configurations. The approach followed and the observations made are presented in the subsequent sections.

2. OVERVIEW OF THE REFERENCE BRIDGE

An overpass bridge along the Egnatia highway of Greece in the location of Pedini [22] is selected as a reference structure for the particular study (Figure 1). The reference bridge consists of a continuous three span box section deck of a total 71.2 m length (19.6 + 32.0 + 19.6), monolithically connected to two circular concrete piers of 8.5m height and 1.7m diameter. The deck consists of an 11 m wide prestressed T-section (i.e., strands with steel grade St 1570/1770, tensile strength of 1770 MPa) with two cylindrical voids of 1.10 m diameter.

In the longitudinal direction, the deck is also supported on the abutment through two ALGAPOT PNm 200 sliding pot bearings. An ALGAFLEX T160 expansion joint ensures that the deck movement will not exceed 12 cm beyond which the abutment-backfill-foundation-embankment system is directly activated. In the transverse direction, stoppers are used to block the lateral movement of the deck and resist seismic forces. This is achieved through ALGAFLON NTm 100 bearings that are used between the deck and the stoppers. Both the abutments and the piers are supported on pile-group foundations.

The bridge was designed for load combinations according to the German Norms (i.e. DIN 1055, 1045, 1072, 1075, 1054, 4227, 4085, 4014) while the seismic design was carried out according to the Greek standards EAK 2000 [23] and E39/99 [24], the first being the Greek Seismic Code for the design of structures (General and Buildings) and the latter the Code for the Seismic Design of Bridges. The bridge site is located in the Seismic Risk Zone I which is equivalent to a peak ground acceleration of $a_g = 0.16g$, while the vertical peak ground acceleration is taken as 0.7 times the horizontal one. The behavior factors of the system were also adopted according to the E39/99 [24] document as: $q_x=2.50$, $q_y=3.50$, $q_z=1.00$ for the three principal directions, respectively [25]. The construction was undertaken on behalf of the Egnatia Highay by Aktor, S.A., Pantechniki S.A. and Themeliodomi S.A. at a cost of 730,000€(2003).
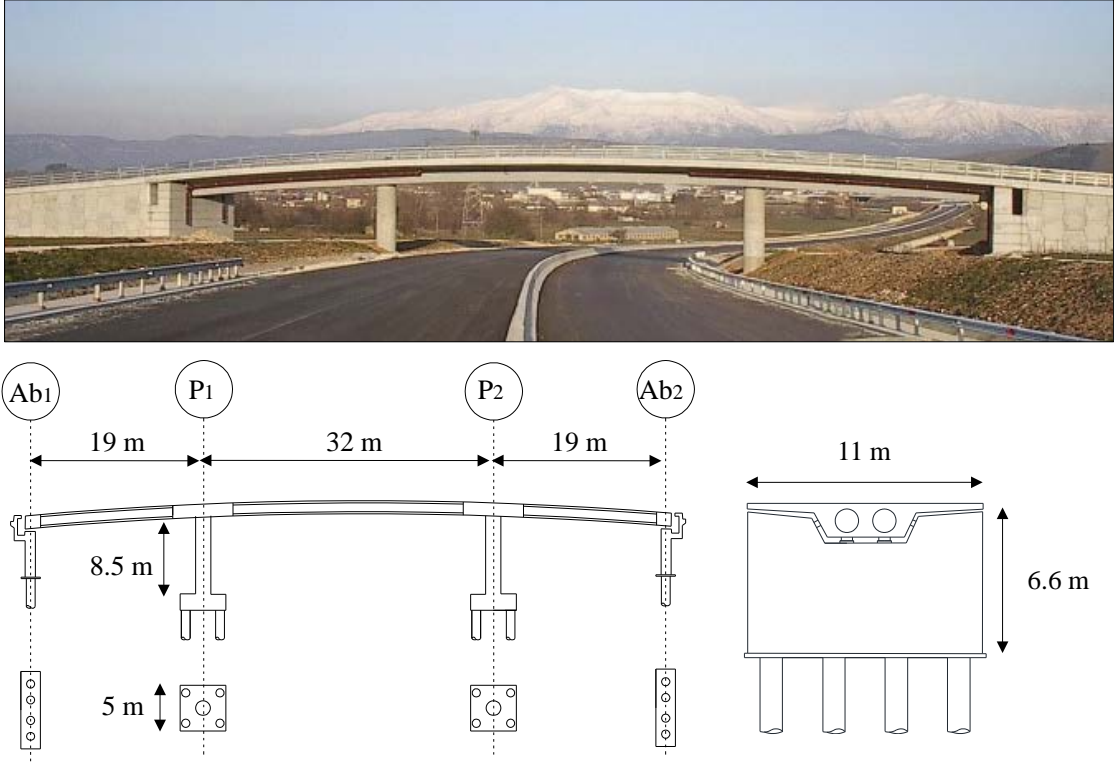

Figure 1: Overview of the Pedini Bridge

The two abutments are founded on a 4x1 pile-group system embedded by 32 m and 28 m, respectively, while the two piers of the bridge are founded on 2x2 pile-groups embedded in 32 and 28 m respectively. The soil properties of the bridge's site are defined by two cohesive soil layers of soft clay and medium density clay respectively, with dense limestone bedrock located below the cohesive layers. The presented information on the actual foundation properties and soil profile of the bridge site will not be exploited in the current study as parametric profiles and subsequently (re-designed) foundation configurations have been deliberately generated to provide a more thorough investigation of the problem. The concrete quality is B35 for piers and

deck according to the German standards of the time (equivalent to C25/30 and C30/37 of Eurocode 2, with average characteristic strength of f_{ck}=27.5MPa, and modulus of elasticity E=31.25 GPa) and B25 for abutments and pile foundations (equivalent to C20/25 of Eurocode 2, with characteristic strength of f_{ck}=20 MPa, and modulus of elasticity E=30 GPa). Concrete density is taken $\rho=2.5$ ton/m^3 and Poisson ratio $v=0.3$.

Modal analysis of the (fixed-based) bridge identified two uncoupled predominant modes of vibration, one, purely translational, transverse with T=0.92sec (mass participation factor ε=95.8%) and one translational, longitudinal mode with T=0.73sec (mass participation factor ε=98.1%) in good agreement with previous studies [22].

3. NUMERICAL MODELING

For the development of the reference bridge FE model two different approaches are followed for considering soil-structure interaction, distinguished in terms of how the frequency-dependent dynamic stiffness matrices are considered. In both cases, the expansion of the substructure method in the time domain is implemented with the overall soil-structure system being divided into two sub-domains with nonlinear and equivalent linear properties, respectively (Figure 2). The first, nonlinear sub-domain consists of the bridge superstructure and piers, which are modeled using the finite element software OpenSees [26] considering both material nonlinearities at the piers (Figure 3), as well as geometrical nonlinearities expected at the lateral deck-abutment joints (Figure 4a). The second, equivalent linear sub-domain includes the abutments, the pier foundations and the semi-infinite soil volume, the dynamic behavior of which is initially extracted in the form of dynamic stiffness in the frequency domain and is then consolidated at the interface level between the bridge and the subsoil.

To comparatively assess the effect of addressing SSI frequency dependence, two different FE models are implemented at the soil-structure interface of piers and abutments interface, involving (a) a conventional Kelvin-Voigt model and (b) the recently developed, impedance function mapping LP model [1].

Due to the expected significance of the site properties in the behavior of the soil-bridge structure system, a breadth of different profiles are parametrically assumed. A group of six different soil profiles are selected with a shear wave velocity $V_{s,30}$ ranging between 100 m/s to 300 m/s, corresponding to both cohesive and cohesionless materials as illustrated in Table 1. It is noted that soil stiffness is assumed constant with depth for clays and parabolically increasing for the case of sands.

Table 1: Properties of the alternative, uniform soil profiles

ID	Soils	G (MPa)	ρ (ton/m^3)	N	C_u (KPa)	φ (°)	$V_{s,30}$ (m/sec)
S1	Soft Clay	13.0	1.3	0.43	20	-	100
S2	Loose Sand	42.5*	1.7	0.34	-	29	170
S3	Medium Clay	60.0	1.5	0.41	40	-	200
S4	Medium Sand	71.25*	1.9	0.33	-	33	260
S5	Hard Clay	150.0	1.8	0.41	70	-	290

(With regard to cohesionless soils, the values of shear moduli correspond to the reference depth of 4m)

4

Table 2: Alternative pier foundation configurations

Soil id	Pile group 2x2			Pile group 3x3		
	L (m)	D (m)	S/D	L (m)	D (m)	S/D
S1	25	1.4	2.9	20.0	1.2	1.7
S2	15	1	4.0	10	0.8	2.5
S3	22	1.2	3.3	15.0	0.8	2.5
S4	15	0.7	5.7	8.0	0.7	2.9
S5	22	0.7	5.7	10.0	0.7	2.9

As the foundation can also greatly influence the impact of soil-structure interaction, different (i.e., 2x2 and 3x3) pile group configurations are designed for each distinct soil condition according to the Eurocode 8 provisions as illustrated in table 2 [27–29]. The design is performed on the basis of the corresponding design actions (i.e., bending moments, shear and axial forces) that resulted from the response spectrum analysis of the superstructure, on the basis of the Eurocode 8 (Soil Class D for S1-S2 and soil Class C for S3-S5). Details on the modeling decisions made for each component of the system are further discussed in the following sections.
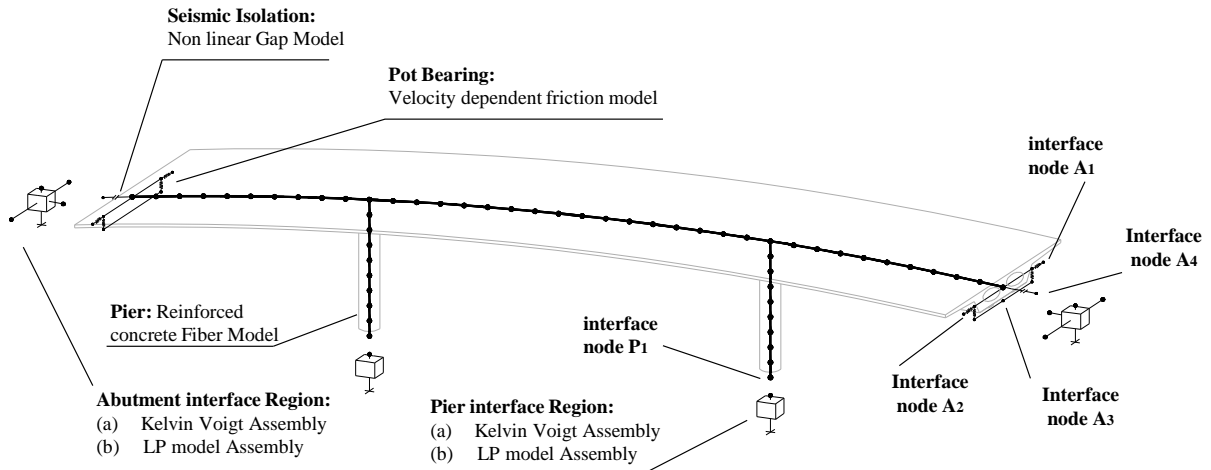

Figure 2: Overview of the sub-structured FE model of the bridge.

3.1 Bridge Superstructure

The deck of the overpass reference bridge is simulated with 3D beam elements according to the OpenSees Element *elasticBeamColumn*. Along the mid-span the deck is modeled with a non-prismatic double cell box section, while a solid section is used at the vicinity of the supports. The bridge deck is considered elastic, as it is prestressed and thus expected to remain uncracked during earthquake loading.

3.2 Bridge Piers

Three-dimensional fiber-section elements with nonlinear uniaxial fiber materials are used for modeling the circular bridge piers according to the OpenSees element *forceBeamColumn*. Given that the piers are capacity-designed and shear failure is unlikely for the design earthquake, the assumption of purely flexural behavior is deemed legitimate. The fiber section discretization is utilized through appropriate fibers located in the three different regions of the section, namely the unconfined concrete, the steel reinforcement and the confined core, respectively (Figure 3, right). The concrete uniaxial materials used for the fiber section simulation are

modeled according to concrete material laws proposed in [30], while a bilinear simplified stress strain behavior is assumed for the reinforcement steel. The nonlinear concrete properties in compression are illustrated in Figure 3a. The moment to curvature relationship of the pier section under the static axial load N=-7.7 MN is illustrated in Figure 3b.
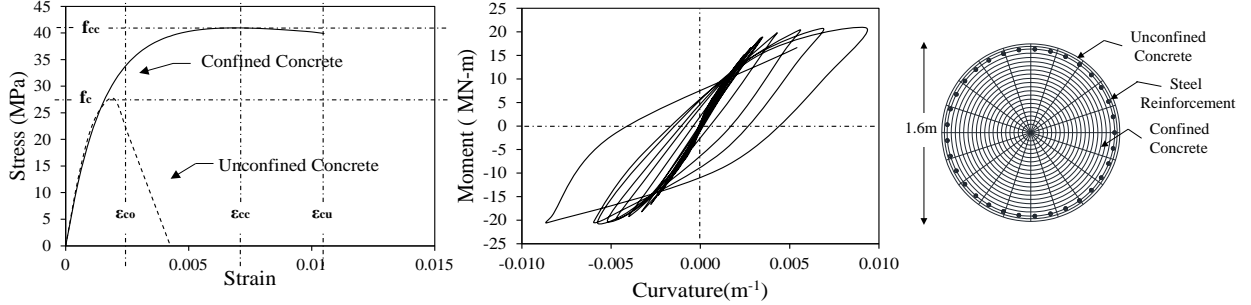

Figure 3: Modeling assumptions for the nonlinear behavior of the bridge piers: concrete stress-strain (σ-ε) relationship (left), section Moment-Curvature (M-φ) curve (middle) and fibre modelling (right).

3.3 Abutment to deck connection

As already mentioned, the deck is longitudinally connected to the abutment through pot sliding bearings and a 12 cm expansion joint, which are modeled through the *flatSliderBearing* (Figure 4,right) and the *ElasticPPGap* (Figure 4, left) nonlinear elements respectively as provided by OpenSees.
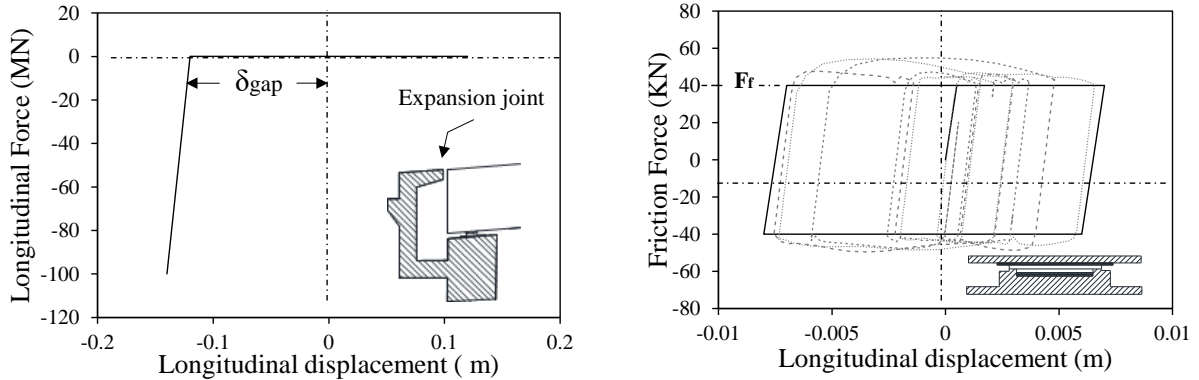

Figure 4: Geometrically nonlinear behavior at the abutment expansion joint (left) and force-displacement relationship of the pot bearings (right).

More precisely, for the purpose of this analysis, the pot sliding bearings of the abutment support are simulated through a velocity and pressure dependent friction model as proposed by Constantinou et al in [31]:

$$F_{fr} = W \cdot (f_{max} - Df \cdot e^{a \cdot \dot{U}}) \tag{1}$$

where a is a constant for given bearing pressure and interface condition, f_{max} is the coefficient of friction at large velocity of sliding (after levering off) and D_f the difference between fmax and the sliding value at a very low velocity. The exponential relation of the velocity to friction coefficient is defined based on experimental data [32] assuming a pure PTFE – stainless steel interface with lubrication, similar to the type 1 Unfilled PTFE interface studied in the particular

6

experimental campaign. The behavior of the bearings according to the selected equation (black color) along with the response of the bearings under a random dynamic excitation (gray color) are illustrated in Figure 4, right.

4. SOIL-STRUCTURE INTERACTION

4.1 Extraction of the soil- foundation domain dynamic stiffness

As the soil structure interaction phenomenon is simulated through the substructure method expansion in the time domain, the calculation of the equivalent linear properties of the condensed segment is an essential step prior to the implementation of the method. The inelastic properties of the soil domain are simulated according to the shear modulus and material damping relationships proposed in [33]. The strain to shear modulus and damping ratio relationships corresponding to each individual soil profile are illustrated in Figure 8 and 9.
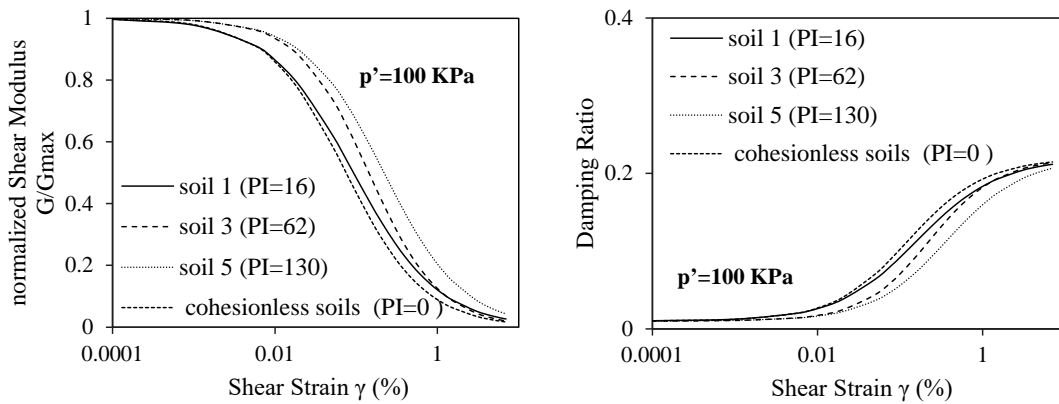

Figure 5: Normalized soil shear modulus to shear strain relationship for the different soil profiles.

One-dimensional site response analysis is performed for each of the selected earthquake ground motion excitations to be used in the foreseen fragility derivation procedure. The equivalent linear soil domain properties are then calculated based on the effective shear strain (i.e., approximately equal to $0.65\gamma_{max}$) observed for each analysis. These equivalent values of the shear modulus G of the soil profile are implemented in the extraction of the impedance function matrices of soil domain segment of the overall system.

In regard to the impedance matrix extraction procedure the overall (equivalent linear) soil volume is divided into four interface regions corresponding to the two abutments and the two piers supports. To reduce the computational effort, essential to the particular case study, the four distinct interface regions are considered to be uncoupled, hence the impedance function matrices are extracted independently for the pier foundation and abutment interface regions. The extraction of the impedance function matrices for the four interface regions is accomplished for the different combinations of soil and foundation types (as defined in Tables 1 and 2).

The pile group foundation dynamic behavior has been thoroughly investigated in the past [34–38], hence, the impedance matrix is generated analytically through the formulation proposed by Gazetas and Makris in [37,38] as implemented by the software ASING [39]. As the selected closed form solution has been evaluated in the past [37,38] through comparison with rigorous solution results of pile group impedance functions, an additional verification is not included within this study.
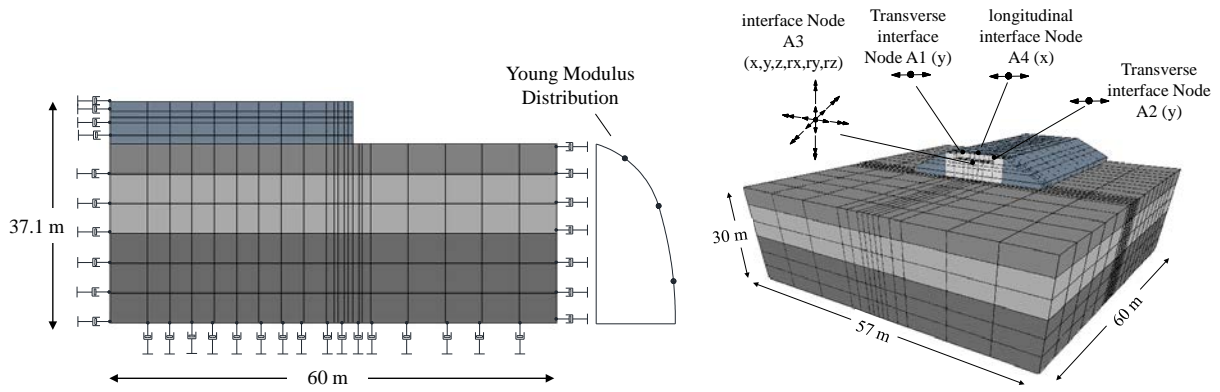
Figure 6: FEM model of the abutment-foundation-embankment domain for the cohesionless soil profiles
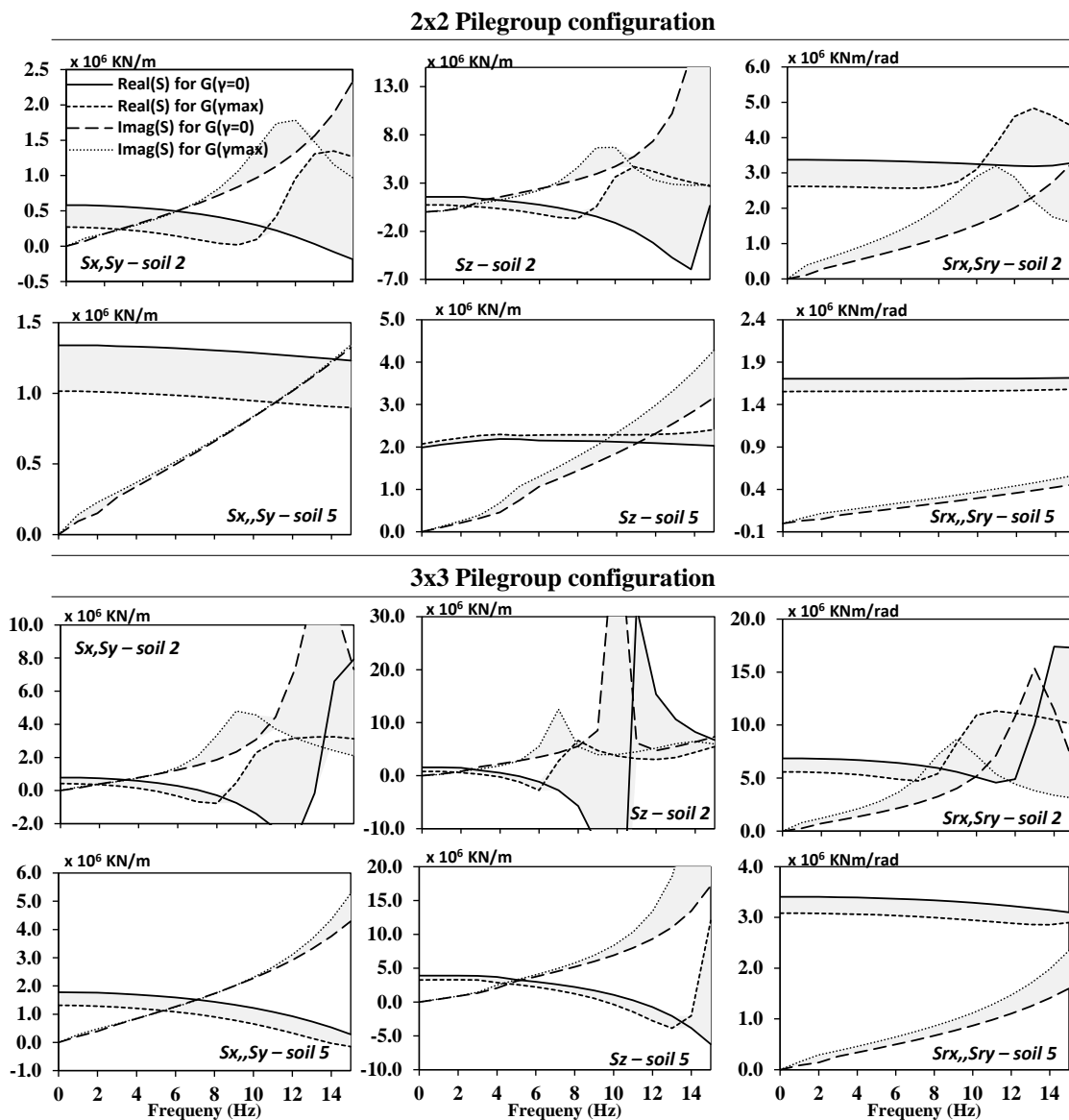

Figure 7: Sample of the generated impedance functions of the pier-foundation-soil interface region for the case of (a) 2x2 pile group and (b) 3x3 pile group configuration

For the foundation-to-pier base connection a 6 DOF interface region is assumed, with non-diagonal matrix terms limited to the rotation-translation coupling behavior. The derived dynamic stiffness matrices of the 2x2 and 3x3 pile groups for soil profile scenarios S2 and S5 are indicatively illustrated in Figure 7 for the extreme cases of the equivalent soil properties corresponding to the elastic strain ($\gamma=0$) and the maximum strain reached during the one dimensional site response analysis(γ_{max}).

On the other hand, the refined FEM model presented in Figure 6b was implemented for deriving the impedance function matrix of the abutment – Embankment – soil interface regions. This was due to the fact that the analytical solutions available do not explicitly account for foundation stiffness, hence, a 3D FE analysis was deemed preferable. The overall FE model consisted of a total number of 2,695 hexahedral brick finite elements comprising a generally coarse mesh refinement. The non-deflecting behavior of the semi-infinite soil domain is achieved through the assignment of damping properties on the external boundary of the truncated FEM domain, according to Lysmer [40], representing a homogeneous half-space beneath the boundaries. The pile group foundation of the abutment has been simulated with one-dimensional elastic beam elements representing each individual pile. The impedance function matrix to be generated is comprised by 9 interface DOFs (also depicted in Figure 6) among which, six correspond to DOFs associated with the permissible movements through the bearing system between the deck and the abutment, while three additional DOFs correspond to the three translational expansion joint regions of the abutment itself.
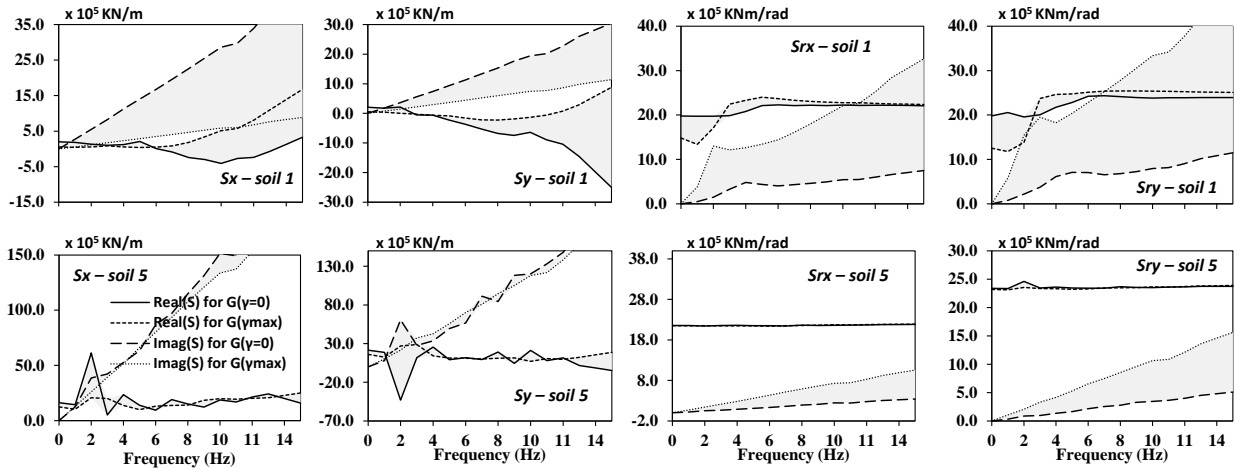

Figure 8: Sample of the generated (target) impedance functions for the abutment-foundation-embankment interface region.

With control over the node and element topology, the 3D FEM model was constructed in the open source finite element software OpenSees, where the overall stiffness matrix was extracted for different equivalent linear properties corresponding to each specific earthquake excitation. The knowledge over the node and element topology of the model made the derivation of the overall mass and damping matrix attainable. As the overall viscous elastic dynamic system is acquired the computationally viable method of dynamic condensation in the frequency domain is selected for the extraction of the impedance matrix of the interface DOFs as illustrated in equation (2).

$$[(\mathbf{K} - \omega^2\mathbf{M}) + i\omega\mathbf{C}]\ \mathbf{U} = \mathbf{F}$$

$$\mathbf{SU} = \mathbf{F}$$

$$\mathbf{S} = \begin{bmatrix} \mathbf{S}_{ii} & \mathbf{S}_{ij} \\ \mathbf{S}_{ji} & \mathbf{S}_{jj} \end{bmatrix}$$

$$\mathbf{S}_{ii}^* = \mathbf{S}_{ii} - \mathbf{S}_{ij}\mathbf{S}_{jj}^{-1}\mathbf{S}_{ji} \tag{2}$$

where $\mathbf{S}$ corresponds to the overall dynamic stiffness matrix of the entire foundation and soil domain. After condensing all DOFs except the DOFs at the interface, the $\mathbf{S}_{ii}^*$ corresponds to the 9x9 impedance function matrix of the abutment interface region. A sample of the impedance functions generated with the aforementioned procedure is illustrated in Figure 8.
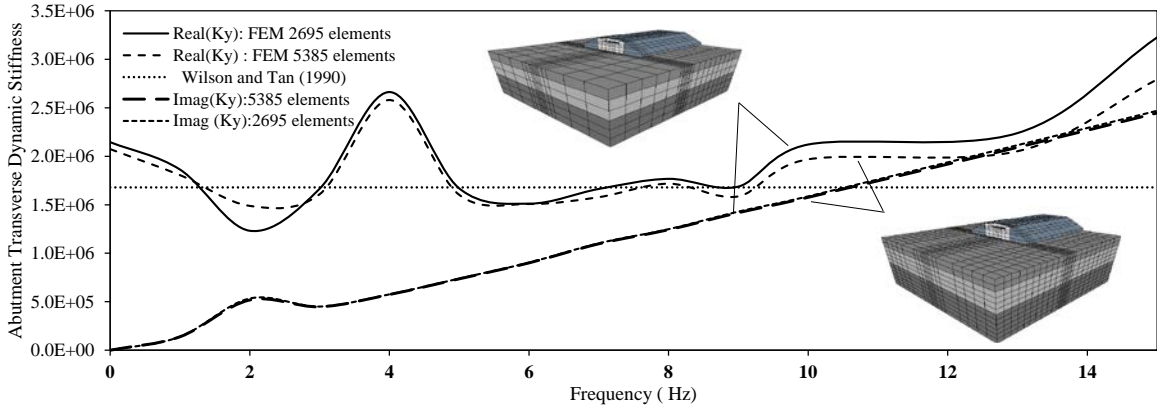

Figure 9: FEM model of the abutment-foundation-embankment domain for the cohesionless soil profiles

The 3D FEM model of the abutment-embankment soil interface was verified by comparing the attained impedance functions for cases of different mesh refinement, as well as with previous studies involving a simplified approach for calculating the static stiffness of the system. In figure 9 the transverse impedance function of the segment in question is illustrated for two different levels of mesh refinement, along with the static transverse stiffness of an embankment according to the wedge model proposed by Wilson and Tan [41]. Since further mesh refinement leads to minor improvement of the resulting impedance functions, the initially defined mesh is considered acceptably accurate.

4.2 Extracted dynamic stiffness integration into the bridge FE model

The impedance function matrices corresponding to the pier foundation and abutment interface regions are integrated on the nonlinear FEM model of the bridge structure through the appropriate dynamic spring assemblies as illustrated in Figure 10. The construction of the dynamic springs of each interface region assembly is accomplished according to the Kelvin – Voigt Model with parameters defined from the impedance function values in the mean frequency f_m (eq. 3) of each excitation (approach 1) and the LP modeling assembly according to [17], calibrated to the overall dynamic stiffness matrices generated in the previous section (approach 2).

$$f_m = \frac{\sum_i C_i^2}{\sum_i C_i^2 (1/f_i)} \tag{3}$$

where C_i are the Fourier amplitude coefficients, f_i are the discrete fast Fourier transform (FFT) frequencies between 0.25 Hz $\leq f_i \leq$ 20 Hz and $\Delta f \leq$ 0.05 Hz is the frequency interval used in the FFT.

It is noted herein that the mean frequency of excitation f_m is used for the parameterization of the frequency-independent Kelvin Voigt model as opposed to the fundamental frequency f_{SSI} of or the pseudo-natural frequency (f_{pSSI}) of the coupled system, the latter defined as the frequency where the ratio of the horizontal displacement of the superstructure us is maximized with respect to the foundation motion up [42] for three main reasons: (a) being a key parameter of the dynamic stiffness of the system, (b) it has been parametrically found as the most efficient alternative in defining frequency-independent Kelvin-Voigt models [21] and (c) given that the site response analysis of the five soil profiles studied is equivalent linear, the fundamental frequency f_{SSI} or f_{pSSI} of each coupled system is effectively intensity-dependent, thus calibrating the K-V model to the frequency of the system would hinder the identification of clear trends.

In regard to the LP dynamic spring formulation, the 3 core LP model illustrated in Figure 10d is selected for the particular study due to the accurate representation and computational efficiency that it has to offer. Sample results of the calibration process for some demanding scenarios are illustrated in Figure 11.
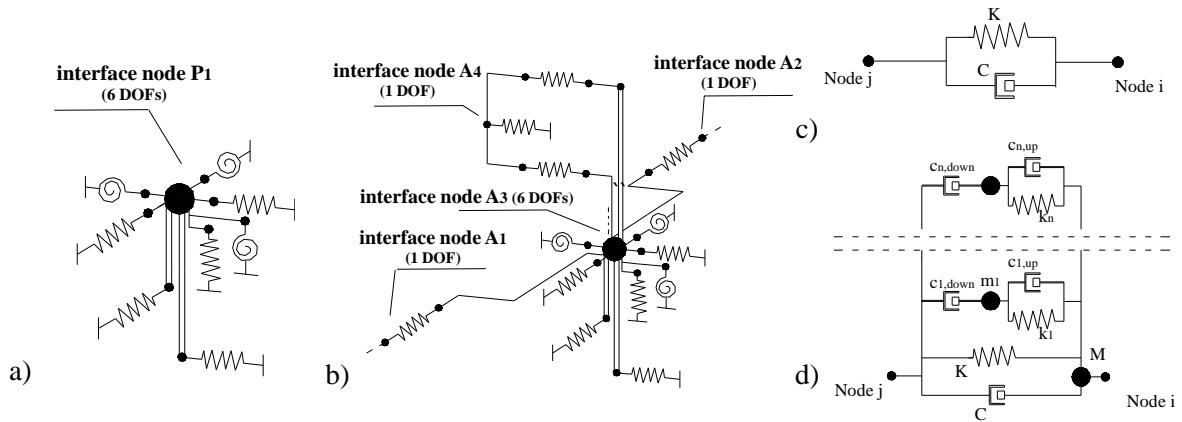
Figure 10: (a) Dynamic spring assembly of the pier-pile group-soil interface region, (b) Dynamic Spring assembly of abutment interface region (c) Dynamic spring as Kelvin-Voigt Model (d) Dynamic spring as LP model

Through the calibration of the extensive number of targeted impedance functions essential to the different configuration and loading scenarios (18,900 for the pier base and 14,390 for the abutment interface regions) some insightful observations have been achieved considering the LP modeling efficiency. For both scenarios of the analytically derived pile-group and the abutment FEM generated impedance functions the implemented LP modeling method is observed to achieve satisfying and consistent results.

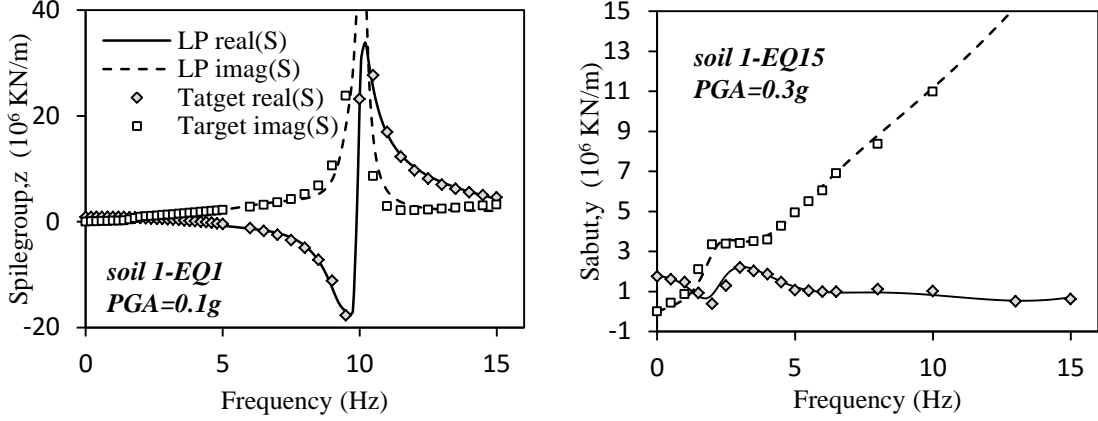Figure 11: Sample of calibration efficiency of the LP models (a) for the pile group and (b) the abutment foundation.

5. FRAGILITY ANALYSIS

The derivation of the fragility curves corresponding to each individual component of the reference bridge structure is performed through the numerical calculation of the conditional probability of the seismic demand exceeding a selected threshold value under a specific magnitude of a selected, efficient and sufficient intensity measure, IM. Assuming a lognormal probability distribution for the representation of the stochastic properties of seismic demand of a structural component, the calculation of the conditional probability is derived as:

$$P_{comp.}[D \geq C \mid IM] = \Phi\left[\frac{\ln(D_m / C)}{\beta_{d|IM}}\right] \tag{4}$$

where the variable D corresponds to the seismic demand of an individual component, C is the value of the corresponding structural limit state for this particular component, IM is the selected intensity measure of the earthquake excitation (typically Peak Ground Acceleration a_g, Spectral Acceleration $S_a(T)$ or Spectral Displacement $S_d(T)$), Φ is the standard normal probability integral, D_m is the median value of the seismic demand D, and $\beta_{d|IM}$ is the logarithmic standard deviation associated with seismic demand. The median seismic demand of the component along with the seismic demand logarithmic deviation are approximated through the regression of simulated data points relating the Intensity Measure adopted to the seismic demand according to the proposed procedure in [43]:

$$D = a \cdot IM^{b} \cdot \varepsilon \tag{5}$$

where a and b are fitting parameters and ε is an error function also expected to follow a lognormal distribution. The training data used for the regression procedure are generated through the nonlinear time history analysis of the reference bridge model under a number of different earthquake excitations.

The multi-damage fragility of the reference bridge at the *system* level is derived according to the assumption that the overall bridge system can reach a specific limit state under the condition that *one or more* individual components have reached the particular limit state [14]. Even though there are some limitations of the particular approach as per the direction of loading [16] the individual fragility curves at the *component* level can be used to estimate an upper or lower bound of the system fragility, under the assumption of a mutually exclusive or uncorrelated

12

component probability relation respectively to the two bounds. As a result, the limit state probability of the overpass bridge studied is obtained, as an upper bound, from the union of probabilities of each individual component in the respective limit state [14], which is calculated herein through a Monte Carlo sampling. Due to the fact that the individual fragility curves at the *component* level follow a lognormal distribution, the system level fragility of the bridge is expected to follow a lognormal distribution as well and as such, the latter is through a regression analysis of the discrete fragility curve points derived from the Monte Carlo simulation.

5.1 Earthquake ground motion selection

The frequency content of the earthquake excitation sample required for the vulnerability analysis is a key parameter, particularly given the overall objective to assess the influence of frequency-dependent soil-structure interaction on the bridge fragility estimations. Three sets of earthquake excitations are formed for the particular study based on their frequency content as expressed by the ratio of their maximum acceleration to their maximum velocity ratio *a/v* [44]. It is recalled that this ratio is not commonly used in ground motion selection for a target seismic hazard, but it is a useful proxy of earthquake magnitude, distance from source and frequency content of the recorded ground motions for cases that a wide sample needs to be formed independently of the particular site in question [45]. The three individual ground motion sets are defined as of low, moderate and high *a/v* ratio, i.e. {*a/v<0.8*, *0.8< a/v <1.2* and *a/v >1.2*} respectively, whereas the latter high ratio corresponds to high magnitude, high frequency ground motions. A single component of all seismic motions is considered, along the longitudinal directions.
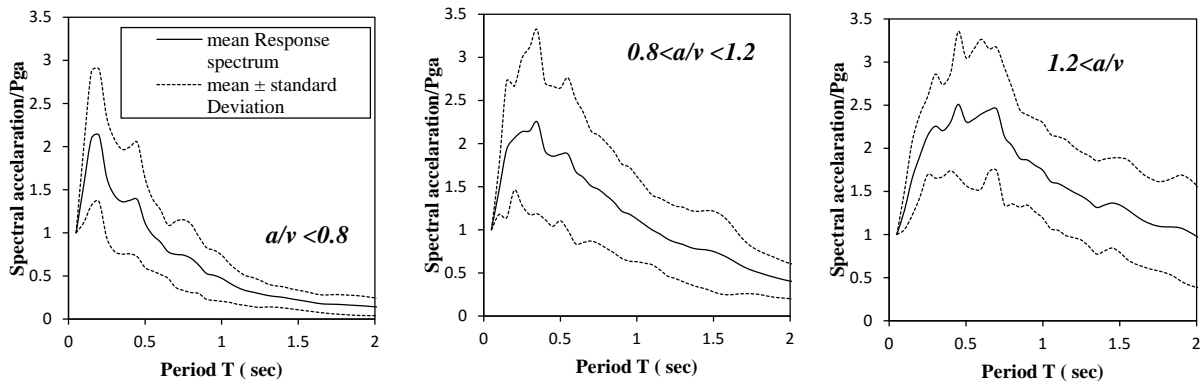

Figure 12: Normalized spectral acceleration of the selected ground motion groups

Selection is limited to ground motions recorded on the soil surface with shear velocity $V_s<300m/s$ in accordance to the alternative soil profiles adopted in this study (Table 1). The earthquake magnitude is further bounded in the range of $5.0< M_w <7.0$, which is kept deliberately wide in order to obtain a more general overview of the influence of ground motion mean frequency. A sample of 45 ground motions is selected (i.e., 15 records per sub-set) and is summarized in Appendix A. Ground motions are scaled in terms of PGA from 0.1g to 0.7g at a step of 0.1g, leading to a sample of 45x7=315 ground motions. The mean value and the standard deviation of the normalized spectral accelerations of each ground motion excitation sub-set are illustrated in Figure 12.

5.2 Definition of capacity limit states for each bridge component

To investigate the potential impact of the simplification made in representing soil-structure-interaction with (frequency-independent) Kelvin-Voigt models it is essential to comparatively assess the seismic demand imposed on each individual structural component of the bridge (i.e., piers and abutment pot bearings) with respect to the more refined Lumped Parameter models developed [1]. Damage at the foundation level and the abutments themselves is not considered herein for simplicity in accordance to the scope of the problem studied; however, it is noted that their damage under certain conditions may potentially affect the fragility at the system level. Three different limit states are considered for each structural component, namely, Serviceability (LS$_1$), Damage Control (LS$_2$) and Collapse Prevention (LS$_3$).

Damage in pier components is introduced in the form of plastic hinges at the two ends of the member (i.e., top and bottom). Since the seismic demand is expected to vary within the structure, and a global response proxy (such as deck displacement or drift for instance) may suppress the localization of demand, a strain- or displacement-based criterion is used to assess damage at each individual structural member. Yielding of the first steel reinforcing bar in tension, initial crushing of the confined concrete and maximum confined concrete strain before hoop rupture are selected as proxies of the LS$_1$, LS$_2$ and LS$_3$ limit states, respectively according to [30]. For the PTFE bearings, damage is expected through the PTFE layer deterioration due to the high velocity cyclic movement in the bearing interface. However, as experimental results on this specific phenomenon are yet inconclusive and no specific deformation thresholds are available, it is only the pot displacement that is taken into consideration. More precisely, closure of the gap (δ_b=12cm) is associated with abutment damage, while an extreme displacement of 17cm is related to pot failure and deck unseating. Threshold values for each limit state are summarized in Table 3.

Table 3. Definition of threshold values of each Bridge Component

Limit State	Threshold Values	
	Strain ε of the bridge pier section	Pot bearing sliding (cm)
Serviceability (LS$_1$)	e_s^a= 0.00250	-
Damage Control (LS$_2$)	e_{cc}^b = 0.00684	δ_b=12 cm=δ_{gap}
Collapse Prevention (LS$_3$)	e_{cu}^c = 0.01040	δ_b=17 cm

[a] *Yielding of reinforcement steel (first yielding of steel in tension)*

[b] *Confined concrete strain of the compression region (maximum moment capacity)*

[c] *Confined concrete strain of the compression region (hoop rupture)*

6. IMPACT OF MODELING SSI FREQUENCY DEPENDENCE ON BRIDGE FRAGILITY ESTIMATES

6.1 Influence on the seismic demand of the bridge components

A total number of 3,150 (315 excitations x 5 soil profiles x 2 foundation configurations) non-linear response history analyses were performed in the particular study, taking into account the different soil profile scenarios both for the 2x2 and 3x3 pile group configuration of the pier foundations. A sample of the mean Engineering Demand Parameters (EDPs) of the individual bridge components is illustrated in the following Figures 13 and 14 for different combinations of soil profile, foundation configuration and ground motion frequency content. The mean engineering demand parameter of each bridge component is approximated through the regression of the simulation generated maximum demand values of each earthquake excitation within a selected excitation group according to equation (5).
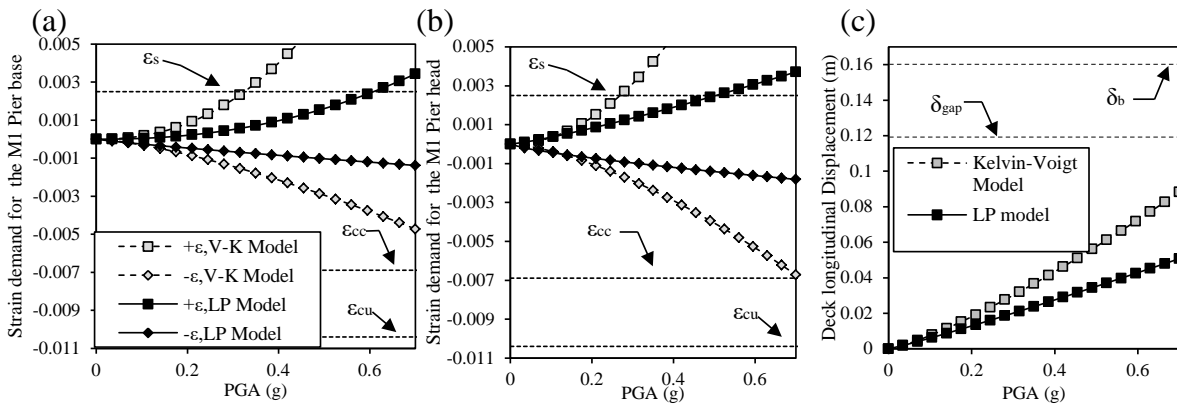

Figure 13: Component strain-based EDP (a) at the pier head, (b) at the pier base (c) at the abutment pot bearings. Scenario of Soft Clay (S1), 3x3 pile configuration and *a/v>1.2*.
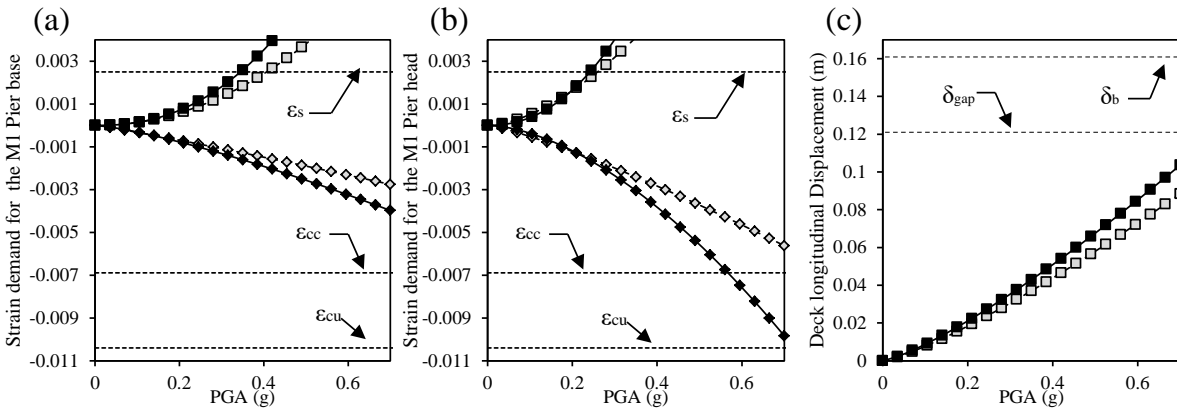
Figure 14: Component strain-based EDP (a) at the pier head, (b) at the pier base (c) at the abutment pot bearings. Scenario of Loose Sand (S2), 3x3 pile configuration and *a/v>1.2*.

A first observation is related to the component seismic demand (in the form of strain-based EDP) for the case of a 3x3 pile group founded within soft clay under near-field ground motions (*a/v>1.2*). More precisely, Figure 13(a) depicts the maximum tensile reinforcement steel strain (+ ε) and compressive concrete strain (- ε) at the section of pier M1 head under the assumption of frequency-independent (Kelvin–Voigt model) and frequency-dependent (L-P model) soil-

structure interaction consideration, respectively. The limit state thresholds ε_s, ε_{cu} and ε_{cc} are illustrated in the form of dashed lines for each one of the three limit states LS_1, LS_2 and LS_3. Similarly, Figure 13(b) depicts the above EDP at pier base, while Figure 13(c) illustrates the displacement associated with the most critical pot bearing. In an identical manner, the same EDPs are plotted versus increasing PGA for the case of soil profile S2 (loose sand), in Figure 14.

What can be clearly seen in both Figures 13 and 14 is that ignoring the frequency-dependence of earthquake ground motion (i.e., adopting the Kelvin Voigt as opposed to LP models to account for SSI effects) may lead to significantly different seismic demand in the form of strain-based EDPs (by a factor that exceeds 2.0 for large values of PGA exceeding 0.3g) both at the piers (base and top) and the abutment bearings. It is also noticeable that the more simplified, K-V model overestimates the strain demand for the case of clay soils while it underestimates the demand for loose sands, even though the frequency content of the ground motions are identical.

The aforementioned distinct difference in the predicted EDPs for the sample motions used can be explained by the fact that the Kelvin-Voigt model represents the targeted dynamic stiffness of the condensed system solely accounted for the excitation mean frequency. Consequently, an error is inevitably introduced as per the dynamic stiffness of the soil-foundation system in all other frequencies. Naturally, the more variant the targeted impedance function with frequency, the higher the error introduced. Whether this simplification will ultimately lead to more or less conservative estimates of seismic demand depends on the interplay between the dynamic characteristics of the soil-foundation system and the properties of the incoming earthquake ground motion. The error produced by the simplified Kelvin-Voigt model approach on the translational DOF impedance function of the pier foundation is illustrated in Figure 15 for the scenarios of (a) a Soft Clay soil profile with the 3x3 pile configuration and (b) a Loose Sand soil profile with the 3x3 pile configuration. In more details the impedance functions of the translational DOF of the pile group foundation under the equivalent linear conditions of $\gamma=0$ are illustrated for the two distinctive simulation methods of the LP and Kelvin-Voigt model. The Fourier amplitude of the Imperial Valley earthquake, measured at the station El Centro Array #9, is also illustrated in both subfigures as an indication of the frequency content of ground motion with $a/v>1.2$

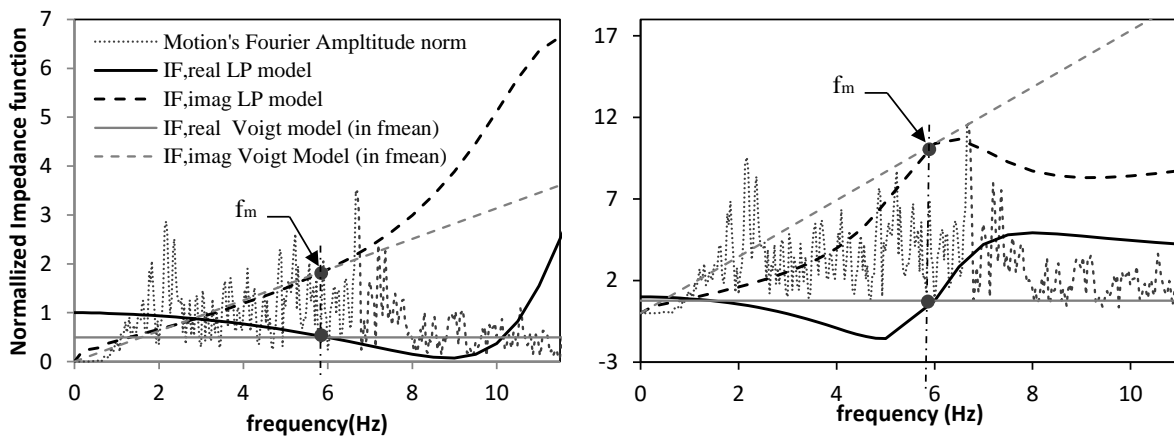Figure 15: Translational Impedance function error of the simplified approach for the scenario of $a/v>1.2$, (a) soft clay and (b) loose sand soil profile

16

In regard to the soft clay soil profile scenario S1 it is observed that the real part of the translational impedance function in question is underestimated for the region of 0-5.93Hz while mainly overestimated for higher frequencies while the imaginary part is underestimated throughout the frequency region of 0-10Hz. As the superstructure will mainly amplify the lower frequency content of the earthquake motion, the dynamic stiffness of the translational spring representing the pile group foundation is expected to be underestimated. On the case of the loose sand soil profile scenario S2, it is observed that on the lower frequency region the translational impedance function spring is overestimated both on the real and imaginary part.

6.2 Impact of SSI frequency dependence on the bridge system fragility

The system level fragility curves of the reference bridge are derived according to the procedure presented in Section *5,* for all the different soil profile scenarios and pier foundation configurations and are illustrated in Figure 16. Each pile group configuration is presented in the form of 10 plots displayed in five rows of different soil profiles (S1 to S5) and two columns of distinct frequency content (*a/v*<0.8 and *a/v*>1.2). Within each plot, six system level fragility curves of the reference bridge are illustrated, corresponding to the three different limit States (LS_1, LS_2 and LS_3) and the two SSI models adopted (Kelvin–Voigt and Lumped Parameter).

By comparing the fragilities predicted in Figure 16 with the Kelvin Voigt and the LP soil-structure interaction models, it is evident that the discrepancies between the two methods are important and increase with increasing IM (particularly for soil profiles S2 to S5). This can be attributed to the fact that higher ground motion intensity leads to nonlinear soil response at specific depths, more complex dynamic behavior of the soil domain and potentially greater variations in the corresponding impedance functions which is in turn reflected on the discrepancy between the frequency-dependent and the frequency-independent models.

In a similar manner, the soil profile and foundation system properties are also found to be a significant influential factor on the accuracy of the simplified frequency-independent approach as they tend to affect the complexity of the targeted impedance thus deviating the fragility estimates. As anticipated, for both pile group configurations (2x2 and 3x3) it is observed that the agreement of the K-V with the more refined LP model is improved for increasing soil stiffness (note that the soil profiles are listed in ascending order of *Vs* from S1 to S5). This is attributed to the fact that for stiffer soils the soil properties have a smaller influence in the behavior of the superstructure, while it is also noticed that the nonlinear phenomena are limited for small-to-moderate intensities and hence, the impedance function does not considerably fluctuate around the mean excitation frequency *fm*, which was used to calibrate the Kelvin-Voigt model in the first place (as an example see Figure 16 for PGA higher than 0.3g). This observation is still valid for the case of the 3x3 pile group foundation, however, due to the subsequent increased complexity of the impedance functions, the fragility estimates under Kelvin-Voigt assumption are distinctly different from those obtained considering the frequency-dependent nature of SSI (LP model) almost for all soil profiles (S1-S4); It is only for the case of stiffer soils (S5) excited by low magnitude, long period motions (*a/v*<0.8) that frequency dependence of the soil-foundation system does not play any role in the predicted system vulnerability as seen in Figure 16(bottom row).
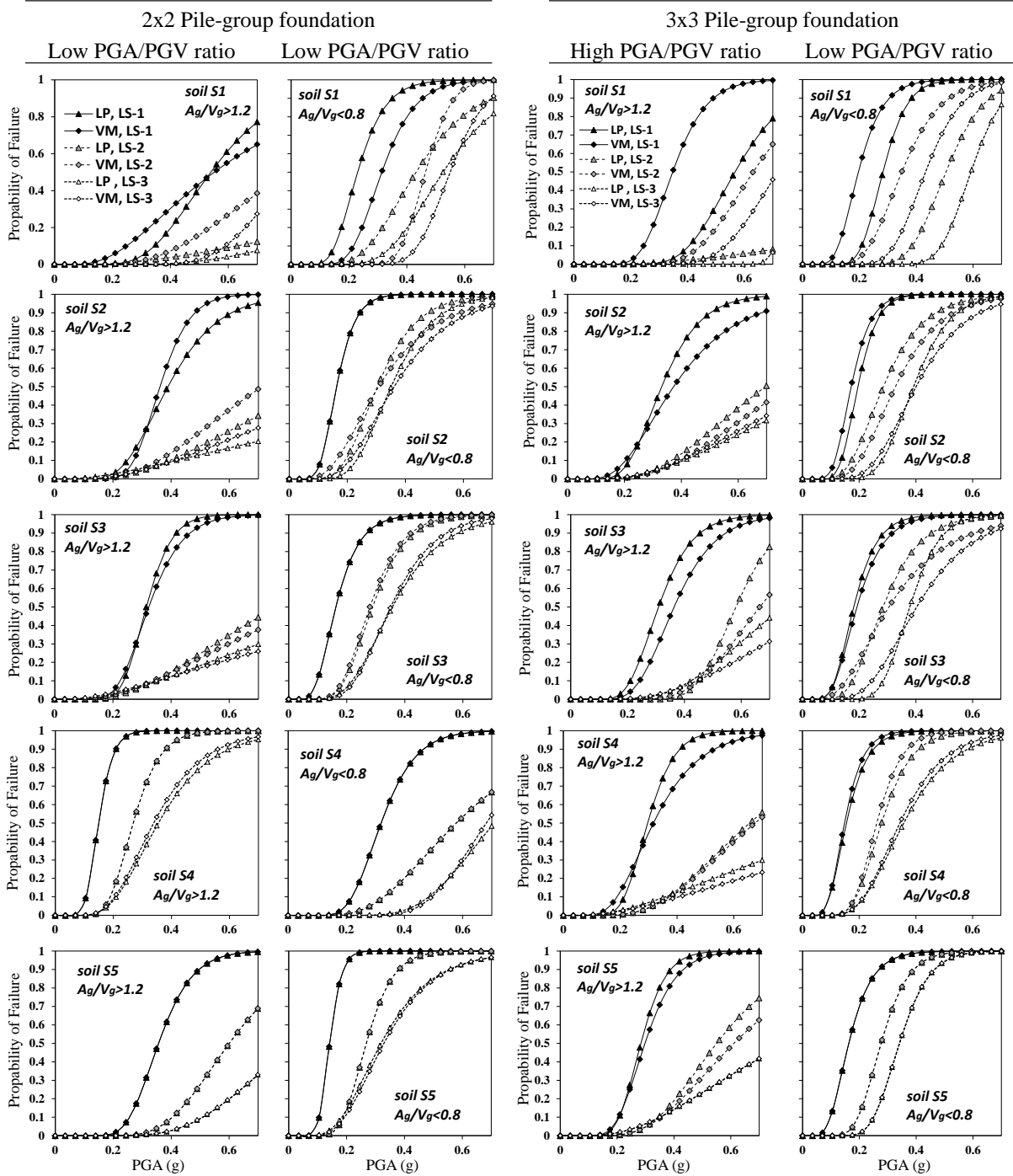
Figure 16: System level fragility curves for the 2x2 pile group formulation and 3x3 pile group configuration.

To better quantify the previously described results, it is essential to define a specific parameter capable of illustrating the overall accuracy error observed in the system fragility curves of the structure due to the use of the frequency independent Kelvin – Voigt method. To that extent the mean absolute percentage error of the conditional probability of the global system surpassing a

specific limit state under the use of the Kelvin – Voigt method (*MAPE*) is appropriately calculated through the following equation (eq. 6) for the different soil profiles, earthquake mean frequency and foundation configuration properties.

$$MAPE = \frac{1}{N} \cdot \sum_{j}^{N} \frac{\left| P_{LSi,System}^{KV}(a_{g,j}) - P_{LSi,System}^{LP}(a_{g,j}) \right|}{P_{LSi,System}^{LP}(a_{g,j})}$$

(6)

where $\min(P_{LSi,System}^{KV}(a_{g,j}), P_{LSi,System}^{LP}(a_{g,j})) \geq 0.05$ and $\max(P_{LSi,System}^{KV}(a_{g,j}), P_{LSi,System}^{LP}(a_{g,j})) \leq 0.95$

The calculated *MAPE* is illustrated in Figure 17 (a),(b) and (c) for the three limit states LS$_1$, LS$_2$ and LS$_3$, respectively. For each plot, the distribution of *MAPE* is presented for both the 2x2 and 3x3 pile group configuration, in relevance to the soil shear velocity $V_{s,30}$ and the earthquake mean frequency f_m.
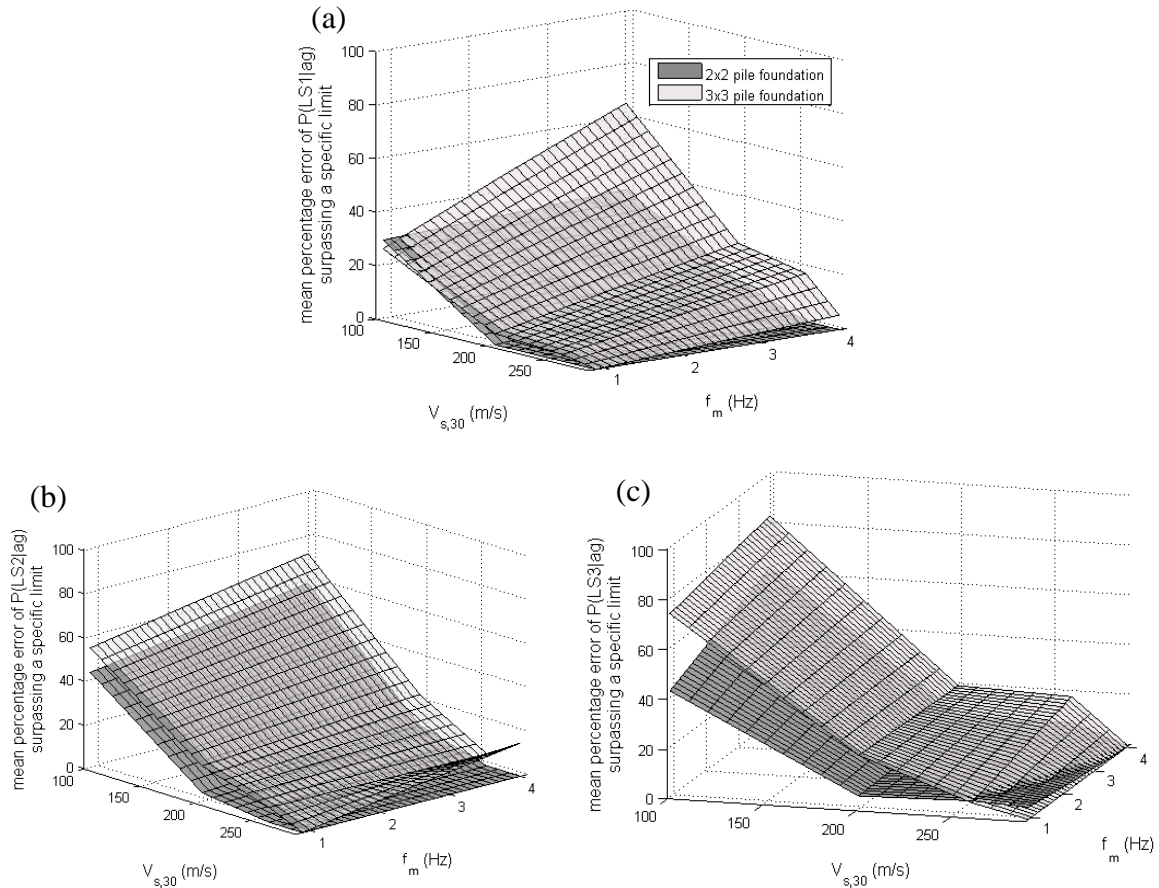
Figure 17: *MAPE* with soil shear wave velocity Vs and the mean frequency f_m of the earthquake excitation for limit states (a) LS1, (b) LS2 and (c) LS3.

As observed in Figure 17(c) for the most critical limit state LS$_3$, the *MAPE* can reach a value of up to 80% and 60% for the 3x3 and 2x2 pile group configurations respectively under the specific conditions of high mean frequency excitation (*f$_m$=4Hz, T=0.25sec*) and a soft soil profile with a shear velocity of $V_{s,30} = 100m/s$. It is also seen that for $V_{s,30} < 200m/s$, *MAPE* remains considerably higher than the value of 20% (for 3x3 pilegroup) and in general higher than 10%

for a 2x2 foundation. For soils with *200m/s<$V_{s,30}$<300m/s*, *MAPE* becomes negligible for the 2x2 pile group systems for the reasons explained in the previous section (i.e., stiff soil conditions combined with minor kinematic interaction that lead to stable impedance functions around the mean frequency of excitation used in the simplified Kelvin-Voight model). The error is again higher for the 3x3 pile group reaching 10-20% for the same reasons, particularly for high to medium frequency content earthquake excitations (*1.5Hz<f_m<4Hz*). As anticipated, the MAPE is lower but still non-negligible for less critical limit states (i.e., L_1 and L_2). More precisely, as shown in Figures 17(a) and 17(b), the maximum *MAPE* for LS$_1$ is 60% and 35% for the 3x3 and 2x2 pile configurations respectively, while for LS2 limit it becomes 70% and 60%. In the majority of the cases studied, *MAPE* tends to be reduced with increasing stiffness, being essentially minimized for *$V_{s,30}$>300m/s*.

7. CONCLUSIONS

This paper investigates the impact of considering (as opposed to neglecting) the inherent frequency dependence of soil-structure interaction on the predicted fragility of RC bridges and quantifies the relevant error introduced in the probability of failure at the soil-bridge system level. An extensive parametric analysis scheme is adopted to comparatively assess the fragility curves generated for the case of a well-studied bridge overpass under simplified (Kelvin-Voigt) and more refined (Lumped Parameter) SSI formulations. The bridge fragility curves have been derived for a number of different parameters such as soil stiffness, earthquake frequency content and foundation configuration. The principal conclusions drawn from this study can be summarized as follows:

(1) The fragility curve miscalculation of a bridge structure due to the use of a frequency independent approach is highly correlated to the soil properties and foundations configuration of the bridge. For the soil profile properties of a mean shear velocity of *$V_{s,30}$ < 200m/s , 200m/s<$V_{s,30}$<300m/s, $V_{s,30}$ > 300m/s* a mean probability percentage error of 20-80% , 10-20% and 0-10% has been respectively observed when a frequency independent SSI approach is incorporated in the simulation. Furthermore, a foundation configuration with a more complex impedance function matrix will lead to a higher mean probability percentage error.

(2) A significant dependence is observed between the frequency content of the earthquake excitation and the fragility curve error generated through the use of a frequency independent approach. A generally higher mean frequency and wider distribution of Fourier amplitude of the earthquake excitation will lead to a higher miscalculation of the bridge fragility curves from the simplified frequency independent method.

(3) It is not possible to predetermine the consequences of the use of a frequency independent method as the actual fragility curves of a bridge structure can be both underestimated or overestimated by the simplified approach.

In conclusion a frequency independent representation of the soil structure interaction of a bridge can lead, under certain circumstances, to a very different bridge behavior from the actual one, and thus may provoke misdirection in the engineer's decision making process.

20

APENDIX A

Earthquake	date	Station	Pga	R	Magnitude	*a/v*
Imperial Valley-01	06/06/1938	El Centro Array #9	0.016	33.2	5	2.59
Northwest Calif-01	09/12/1938	Ferndale City Hall	0.108	54.9	5.5	1.78
Northwest Calif-03	10/08/1951	Ferndale City Hall	0.107	56.0	5.8	2.01
Northern Calif-04	06/06/1960	Ferndale City Hall	0.069	58.8	5.7	1.60
Parkfield	06/28/1966	Cholame - Shandon Array #8	0.264	34.0	6.19	2.29
Northern Calif-05	12/10/1967	Ferndale City Hall	0.190	29.7	5.6	1.99
San Fernando	02/09/1971	Anza Post Office	0.032	188.0	6.61	1.91
Friuli, Italy-01	05/06/1976	Conegliano	0.059	89.6	6.5	1.51
Tabas, Iran	09/16/1978	Ferdows	0.108	117.7	7.35	1.53
Coyote Lake	08/06/1979	Gilroy Array #2	0.294	10.9	5.74	1.45
Norcia, Italy	09/19/1979	Spoleto	0.042	18.2	5.9	2.41
Imperial Valley-06	10/15/1979	SAHOP Casa Flores	0.357	12.4	6.53	1.59
Anza (Horse Canyon)-01	02/25/1980	Anza Fire Station	0.071	15.9	5.19	2.37
Mammoth Lakes-01	05/25/1980	Long Valley Dam (Upr L Abut)	0.340	12.7	6.06	1.87
Taiwan SMART1(33)	06/12/1985	SMART1 O07	0.053	44.7	5.8	1.86
Kern County	07/21/1952	LA - Hollywood Stor FF	0.05	118.3	7.36	0.71
Northern Calif-02	09/22/1952	Ferndale City Hall	0.07	43.8	5.2	1.23
Hollister-02	04/09/1961	Hollister City Hall	0.07	18.9	5.5	0.88
San Fernando	02/09/1971	2516 Via Tejon PV	0.03	71.1	6.61	0.88
Managua, Nicaragua-02	12/23/1972	Managua, ESSO	0.29	5.7	5.2	1.03
Friuli, Italy-02	09/15/1976	Buia	0.11	17.1	5.91	0.96
Tabas, Iran	09/16/1978	Dayhook	0.35	20.6	7.35	1.24
Coyote Lake	08/06/1979	Gilroy Array #3	0.26	9.6	5.74	1.16
Imperial Valley-06	10/15/1979	Aeropuerto Mexicali	0.34	2.5	6.53	1.13
Mammoth Lakes-03	05/25/1980	Convict Creek	0.22	5.9	5.91	1.24
Corinth, Greece	02/24/1981	Corinth	0.26	19.9	6.6	1.04
Mammoth Lakes-10	01/07/1983	Convict Creek	0.17	8.9	5.34	1.09
Coalinga-01	05/02/1983	Parkfield - Cholame 4AW	0.07	58.5	6.36	1.14
Lazio-Abruzzo, Italy	05/07/1984	Roccamonfina	0.04	47.4	5.8	1.02
Hollister-04	01/26/1986	Hollister Diff Array #1	0.11	14.8	5.45	1.15
Northern Calif-03	12/21/1954	Ferndale City Hall	0.19	30.8	6.5	0.69
El Alamo	02/09/1956	El Centro Array #9	0.05	121.2	6.8	0.70
Borrego Mtn	04/09/1968	LA - Hollywood Stor FF	0.01	226.8	6.63	0.41
San Fernando	02/09/1971	Bakersfield - Harvey Aud	0.01	117.6	6.61	0.47
Friuli, Italy-02	09/15/1976	Codroipo	0.02	46.7	5.91	0.84
Tabas, Iran	09/16/1978	Boshrooyeh	0.11	74.7	7.35	0.56
Imperial Valley-06	10/15/1979	Chihuahua	0.27	18.9	6.53	0.92
Coalinga-01	05/02/1983	Parkfield - Cholame 1E	0.09	54.6	6.36	0.82
Taiwan SMART1(25)	09/21/1983	SMART1 I01	0.03	99.3	6.5	0.73
Borah Peak, ID-02	10/29/1983	BOR	0.07	18.0	5.1	0.93
Morgan Hill	04/24/1984	Agnews State Hospital	0.03	24.9	6.19	0.68
Taiwan SMART1(40)	05/20/1986	SMART1 C00	0.20	68.2	6.32	0.80

N. Palm Springs	07/08/1986	Morongo Valley	0.21	6.3	6.06	0.57
Chalfant Valley-02	07/21/1986	Tinemaha Res. Free Field	0.04	57.1	6.19	0.84
Taiwan SMART1(45)	11/14/1986	SMART1 C00	0.14	76.2	7.3	0.48

REFERENCES

1. Lesgidis N, Kwon OS, Sextos AG. A time-domain seismic SSI analysis method for inelastic bridge structures through the use of a frequency-dependent lumped parameter model. *Earthquake Engineering & Structural Dymamics* 2015; **44**(13): 2137–2156. DOI: 10.1002/eqe.

2. Mylonakis GE, Gazetas G. Seismic soil-structure interaction: beneficial or detrimental? *Journal of Earthquake Engineering* 2000; **4**(3): 277–301.

3. Saitoh M. Simple model of frequency-dependent impedance functions in soil-structure interaction using frequency-independent elements. *Journal of Engineering Mechanics* 2007; **133**: 1101–1114.

4. Wolf JP, Preisig M. Dynamic stiffness of foundation embedded in layered halfspace based on wave propagation in cones. *Earthquake Engineering and Structural Dynamics* 2003; **32**(7): 1075–1098.

5. Makris N, Badoni D, Delis E, Gazetas G. Prediction of Observed Bridge Response with Soil-Pile-Structure Interaction. *Journal of Structural Engineering, ASCE* 1994; **120**(10): 2992–3011.

6. Varun V, Assimaki D, Gazetas G. A simplified model for lateral response of large diameter caisson foundations—Linear elastic formulation. *Soil Dynamics and Earthquake Engineering* 2009; **29**(2): 268–291. DOI: 10.1016/j.soildyn.2008.02.001.

7. Stewart JP, Fenves G, Seed RB. Seismic Soil-Structure Interaction in buildings II: Empirical Findings. *Journal of Geotechnical and Geoenvironmental Engineering* 1999; **125**(1): 38–48.

8. Star LM, Eeri M, Givens MJ, Nigbor RL, Stewart JP. Field-Testing of Structure on Shallow Foundation to Evaluate Soil-Structure Interaction Effects 2015; **31**(4): 2511–2534. DOI: 10.4231/D3NK3658M.

9. Sextos AG, Pitilakis KD, Kappos AJ. Inelastic dynamic analysis of RC bridges accounting for spatial variability of ground motion, site effects and soil-structure interaction phenomena. Part 1: Methodology and analytical tools. *Earthquake Engineering & Structural Dynamics* 2003; **32**(4): 607–627. DOI: 10.1002/eqe.241.

10. Mackie KR, Lu J, Elgamal A. Performance-based earthquake assessment of bridge systems including ground-foundation interaction. *Soil Dynamics and Earthquake Engineering* 2012; **42**: 184–196. DOI: 10.1016/j.soildyn.2012.05.023.

11. Kwon OS, Elnashai AS. Fragility analysis of a highway over-crossing bridge with consideration of soil–structure interactions. *Structure and Infrastructure Engineering* 2010; **6**(1-2): 159–178. DOI: 10.1080/15732470802663870.

12. Grange S, Botrugno L, Kotronis P, Tamagnini C. The effects of Soil-Structure Interaction on a reinforced concrete viaduct. *Earthquake Engineering & Structural Dynamics* 2011; **40**(1): 93–105. DOI: 10.1002/eqe.1034.

13. Pecker A, CHatzigogos T. Non linear soill structure interaction impact on the seismic response of structures. *XIV European Conference on Earthquake Engineering*, 2010.

14. Nielson BG, DesRoches R. Seismic fragility methodology for highway bridges using a component level approach. *Earthquake Engineering and Structural Dynamics* 2007; **36**(6): 823–839. DOI: 10.1002/eqe.655.

15. Padgett JE, Desroches R. Sensitivity of Seismic Response and Fragility to Parameter Uncertainty. *Journal of Structural Engineering* 2007; **133**(12): 1710–1718.

16. Taskari O, Sextos AG. Multi-angle, multi-damage fragility curves for seismic assessment of bridges. *Earthquake Engineering & Structural Dynamics* 2015; **44**(13): 2281–2301. DOI: 10.1002/eqe.2584.

17. Wolf JP, Somaini D. Approximate dynamic model of embedded foundation in time domain. *Earthquake Engineering & Structural Dynamics* 1986; **14**(December 1985): 683–703.

18. Wolf JP. Consistent lumped parameter models for unbounded *Engineering & Structural Dynamics* 1991; **32**(December 1989): 11–32.

19. Wu WH, Lee WH. Systematic lumped-parameter models for foundations based on polynomial-fraction approximation. *Earthquake Engineering & Structural Dynamics* 2002; **31**(7): 1383–1412. DOI:

22

10.1002/eqe.168.

20. Du X, Zhao M. Stability and identification for rational approximation of frequency response function of unbounded soil. *Earthquake Engineering & Structural Dynamics* 2010(July 2009): 165–186. DOI: 10.1002/eqe.

21. Saitoh M. On the performance of lumped parameter models with gyro-mass elements for the impedance function of a pile-group supporting a single-degree-of-freedom system. *Earthquake Engineering & Structural Dynamics* 2012; **41**(4): 623–641. DOI: 10.1002/eqe.1147.

22. Moschonas IF, Kappos AJ. Assessment of concrete bridges subjected to ground motion with an arbitrary angle of incidence: static and dynamic approach. *Bulletin of Earthquake Engineering* 2012: 1–25. DOI: 10.1007/s10518-012-9395-2.

23. Earthquake Planning and Protection Organization (EPPO). Greek Seismic Code EAK2000 (amended in 2003), Athens, Greece (in Greek) 2000.

24. Ministry of Public Works of Greece. *Circular E39/99: Guidelines for Seismic Design of Bridges, Athens (in Greek)*. 1999.

25. Kappos AJ, Potikas P, Sextos AG. Seismic assessment of an overpass bridge accounting for non-linear material and soil response and varying boundary conditions. *ECCOMAS Thematic Conference on Computational Methods in Structural Dynamics and Earthquake Engineering, COMPDYN 2007, Rethymnon, Greece*, 2007.

26. McKenna F, Fenves G. *Open system for earthquake engineering simulation, Pacific Earthquake Engineering Research Center, Berkeley, California http://opensees.berkeley.edu.* 2004.

27. CEN. *European Standard EN 1998-1. Eurocode 8: Design of structures for earthquake resistance, Part 1: General rules, seismic actions and rules for buildings", Committee for Standarization*. vol. 3. Brussels, Belgium: European Committee for Standardization; 2004.

28. CEN. *European Standard EN 1998-5. Eurocode 8: Design of structures for earthquake resistance – Part 5: Foundations, retaining structures and geotechnical aspects, Committee for Standarization*. vol. 5. Brussels, Belgium: 2004.

29. CEN. *European Standard EN 1997-1-1: Geotechnical Design. Part 1.1: General rules, Committee for Standarization*. vol. 3. Brussels, Belgium: 2004.

30. Mander JB, Priestley MJN, Park R. Theoretical Stress Strain Model for Confined C *Structural Engineering* 1988; **114**(8): 1804–1826. DOI: 10.1061/(ASCE)0733-9445(1988)114:8(1804).

31. Constantinou MC, Mokha A, Reinhorn AM. Teflon Bearings in Base Isolation II: Modeling. *Journal of Structural Engineering* 1990; **116**(2): 455–474. DOI: 10.1061/(ASCE)0733-9445(1990)116:2(455).

32. Mokha A, Constantinou MC, Reinhorn AM. Teflon Bearings in Base Isolation I: Testing. *Journal of Structural Engineering* 1990; **116**: 438–454. DOI: 10.1061/(ASCE)0733-9445(1990)116:2(438).

33. Zhang J, Andrus RD, Juang CH. Normalized Shear Modulus and Material Damping Ratio Relationships. *Journal of Geotechnical and Geoenvironmental Engineering* 2005; **131**(4): 453–464. DOI: 10.1061/(ASCE)1090-0241(2005)131:4(453).

34. Mylonakis GE, Nikolaou S, Gazetas G, Nikolaou A. Soil-pile-bridge seismic interaction: kinematic and inertial effects. part I: soft soil. *Earthquake Engineering and Structural Dynamics* 1997; **26**: 337–359.

35. Taherzadeh R, Clouteau D. Simple formulas for the dynamic stiffness of pile groups. *Earthquake* 2009(May): 1665–1685. DOI: 10.1002/eqe.

36. Sextos AG, Mylonakis GE, Mylona EKV. Rotational excitation of bridges supported on pile groups in soft liquefiable soil deposits. *Computers & Structures* 2015. DOI: http://dx.doi.org/10.1016/j.compstruc.2015.02.013.

37. Makris N, Gazetas G. Dynamic pile-soil-pile interaction. Part II: Lateral and seismic response. *Earthquake Engineering & Structural Dynamics* 1992; **21**(August 1991): 145–162.

38. Gazetas G, Makris N. Dynamic pile-soil-pile interaction. Part I: analysis of axial vibration. *International Journal of Rock Mechanics and Mining Sciences & Geomechanics Abstracts* 1991; **28**(August 1989): A251–A252. DOI: 10.1016/0148-9062(91)91019-N.

39. Sextos AG, Kappos AJ, Pitilakis KD. Inelastic dynamic analysis of RC bridges accounting for spatial variability of ground motion, site effects and soil-structure interaction phenomena. Part 2: Parametric study. *Earthquake Engineering & Structural Dynamics* 2003; **32**(4): 629–652. DOI: 10.1002/eqe.242.

40. Lysmer J, Kuhlemeyer RL, Kulemeyer RL. Finite dynamic model for infinite media. *Journal of the Engineering Mechanics Division* 1969; **95**(4): 759–877.

41. Wilson JC, Tan BS. Bridge Abutments: Formulation of Simple Model for Earthquake Response

Analysis. *Journal of Engineering Mechanics, ASCE* 1990; **116**(8): 1828–1837.

42. Rovithis E, Pitilakis KD, Mylonakis GE. Seismic analysis of coupled soil-pile-structure systems leading to the definition of a pseudo-natural SSI frequency. *Soil Dynamics and Earthquake Engineering* 2009; **29**(6): 1005–1015. DOI: 10.1016/j.soildyn.2008.11.005.

43. Cornell CA, Jalayer F, Hamburger RO, Foutch DA. Probabilistic Basis for 2000 SAC Federal Emergency Management Agency Steel Moment Frame Guidelines. *Journal of Structural Engineering* 2002; **128**(4): 526–533. DOI: 10.1061/(ASCE)0733-9445(2002)128:4(526).

44. Tso WK, Zhu TJ, Heidebrecht AC. Engineering implication of ground motion A / V ratio. *Soil Dynamics and Earthquake Engineering* 1992; **11**: 133–144.

45. Katsanos EI, Sextos AG, Manolis GD. Selection of earthquake ground motion records: A state-of-the-art review from a structural engineering perspective. *Soil Dynamics and Earthquake Engineering* 2010; **30**(4): 157–169. DOI: 10.1016/j.soildyn.2009.10.005.